IEEE Photonics Journal
An IEEE Photonics Society Publication

Open Access

Demonstration of 108 Gb/s Duo-Binary PAM-8 Transmission and the Probabilistic Modeling of DB-PAM-M BER

Volume 13, Number 1, February 2021

Md Ghulam Saber, *Member, IEEE*
Ramón Gutiérrez-Castrejón, *Member, IEEE*
Zhenping Xing
Md Samiul Alam
Eslam El-Fiky
Daniel E. Ceballos-Herrera
Fabio Cavaliere
Gemma Vall-Llosera
Stephane Lessard
David V. Plant, *Fellow, IEEE*

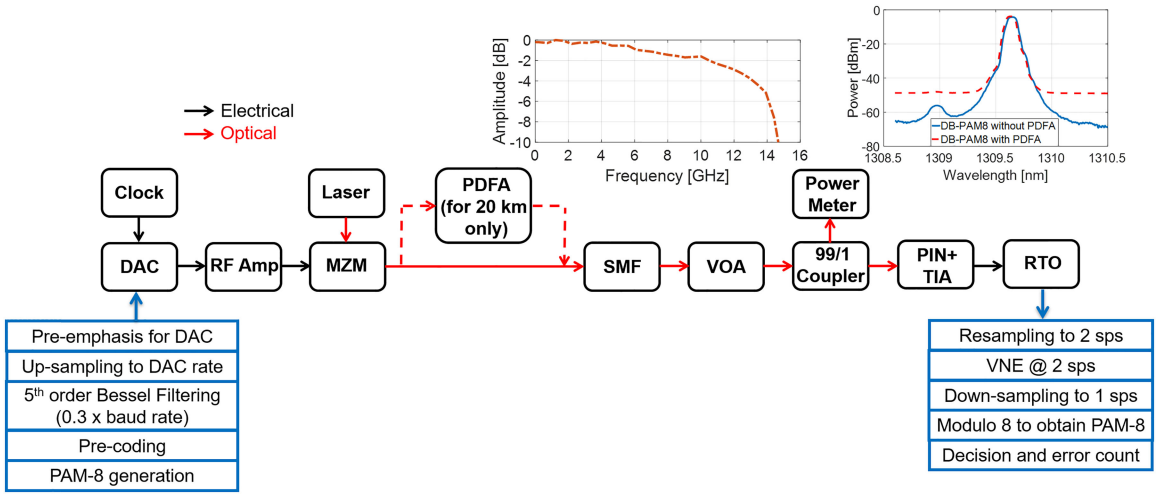

DOI: 10.1109/JPHOT.2021.3054240

Demonstration of 108 Gb/s Duo-Binary PAM-8 Transmission and the Probabilistic Modeling of DB-PAM-M BER

Md Ghulam Saber [1], ***Member, IEEE***,
Ramón Gutiérrez-Castrejón [1,2], ***Member, IEEE***, **Zhenping Xing** [1],
Md Samiul Alam [1], **Eslam El-Fiky** [1],
Daniel E. Ceballos-Herrera [2], **Fabio Cavaliere** [3],
Gemma Vall-Llosera, [4] **Stephane Lessard,** [5]
and David V. Plant, [1] ***Fellow, IEEE***

[1]Department of Electrical and Computer Engineering, McGill University, Montreal, QC H3A 0E9, Canada
[2]Institute of Engineering, Universidad Nacional Autónoma de México UNAM, Cd. Universitaria, 04510 Mexico City, Mexico
[3]Ericsson, Pisa 56124, Italy
[4]Ericsson Research, Ericsson AB, Stockholm 16480, Sweden
[5] Ericsson, Saint-Laurent, Montreal, QC H4S 0B6, Canada

DOI:10.1109/JPHOT.2021.3054240

Manuscript received December 30, 2020; revised January 18, 2021; accepted January 21, 2021. Date of publication January 25, 2021; date of current version February 16, 2021. This work was supported in part by Fonds de Recherche - Nature et Technologies Québec (PBEEE V1 Dossier # 200755) and SPIE Optics and Photonics Education Scholarship (2017, 2018 & 2019), in part by IEEE Photonics Society Graduate Student Fellowship (2019), and in part by the Dirección General de Asuntos del Personal Académico, UNAM, Mexico through PAPIIT project IN103720. *(Md Ghulam Saber and Ramón Gutiérrez-Castrejón contributed equally to this work.)* Corresponding authors: Md Ghulam Saber; Ramón Gutiérrez-Castrejón (e-mail: md.saber@mail.mcgill.ca; rgutierrezc@iingen.unam.mx).

Abstract: We report 108 Gb/s Duo-Binary PAM-8 (DB-PAM-8) transmission using direct-detection aided by Volterra equalizer. The bit-error-rate (BER) performance of the DB-PAM-8 signal has been evaluated through error counting by varying the bit rate, received optical power, and reach. The experimental results suggest that up to 108, 102, and 84 Gb/s signals can be propagated in back-to-back (B2B), and over 10, and 20 km of standard single-mode fiber (SMF), respectively, below the low-density parity-check forward error correction (LDPC-FEC) threshold. Furthermore, we derive a probabilistic model of the BER for multilevel DB-PAM-M signaling that is verified using our measurements. The model of this important performance metric turned out to be accurate enough, especially at low BER values, where its use is more convenient.

Index Terms: Duo-binary PAM-8, IM/DD, optical communication, partial response signaling, short reach, silicon photonics, Volterra.

1. Introduction

To meet the ever-increasing bandwidth demand fueled by the emerging cloud and mobile applications, the capacity of short-reach optical communication network needs a significant increase [1]–[3]. Due to the simplicity of implementation and low-cost, intensity-modulation and direct-detection (IM/DD)-based architectures are preferred to meet the demand of short-reach applications. Several

advanced modulation formats such as pulse amplitude modulation (PAM) [4]–[6], discrete multi-tone (DMT) [4], [7]–[9], and carrierless amplitude and phase modulation (CAP) [10], [11], have been studied in the past using the IM/DD paradigm. Among them, PAM has garnered the most attention due to its ease of implementation and lower power consumption compared to DMT and CAP formats [5], [12]–[15].

High-order modulation formats such as PAM-4 and PAM-8 provide better spectral efficiency and increased capacity per channel. This allows the use of low-bandwidth opto-electronic components to achieve higher capacity. Nevertheless, technical challenges arise when the system is pushed into marginal operating conditions limiting the overall performance. A major source of the transmission impairment is the electrical and opto-electronic bandwidth limitation of the components, including digital-to-analog coverters (DACs), RF amplifiers, modulators, and photodetectors. Inter-symbol interference (ISI) is introduced due to the bandwidth limitation of these components. Another source of distortion is the nonlinearity of the RF amplifiers and the MZMs [16]. This issue is more prevalent in silicon MZMs compared to lithium niobate ones since the phase shifters in silicon MZMs do not behave linearly as a function of the applied voltage [17]. The combined effect of ISI and the nonlinear distortion cannot be compensated entirely using linear equalizers [18]. Especially, for high-order modulation formats such as PAM-8, the impact is more pronounced due to the reduced distance between symbols (amplitude levels).

Bandwidth-efficient partial-response signaling, also known as duo-binary modulation, can be adopted in multi-level PAM modulation formats to increase the per channel capacity further without requiring higher bandwidth components due to the narrow bandwidth of the signal [19]. Furthermore, the duo-binary PAM-M modulation is more resilient to the fiber chromatic dispersion compared to the traditional PAM-M formats [5]. This allows the transmission of higher bit rate signals using a physical layer infrastructure designed for a less demanding scenario, and maintaining the reach at higher bit rates without adopting dispersion compensation techniques. Hence, the duo-binary PAM-M formats enable the operators to increase the network capacity in a quicker manner since the system bandwidth can generate the duo-binary PAM-M signal without any hardware change at the transmitter and a simple change of the threshold and decision circuit at the receiver. This reduces the implementation cost as well since the operators can increase network capacity without any major upgrades to the existing infrastructure. Of course, PAM-M performs better if the system bandwidth is sufficiently ample and the duo-binary PAM-M format is more sensitive to noise compared to the PAM-M counterpart. However, it should be noted that there are always trade-offs, and the solutions need to be chosen based on the overall requirements of the respective applications. Recently, there has been a considerable amount of studies on duo-binary modulation, especially for the two- and four-level PAM formats [20]–[23]. Researchers have studied the PAM-8 modulation format extensively as well [24]–[26]. However, reports about investigations on the performance of DB-PAM-8 modulation within an optical communications context are rather scarce. In [27], 3-Dimensional PAM-8 and DB-PAM-8 modulation were demonstrated reaching up to 200 and 240 Gb/s gross rate, respectively, using high bandwidth components. The generation of the 3-Dimensional format is complex and cannot be done without a digital-to-analog converter/ arbitrary waveform generators.

In this paper, we experimentally demonstrate 108 Gb/s DB-PAM-8 transmission using a system having 12 GHz 3-dB bandwidth in the O-band. O-band is increasing in popularity among different standardization bodies, e.g., IEEE P802.3ca 50 G EPON and IEEE P802.3bs 400 Gb/s Ethernet Task Force, and we envision that the 100 G EPON will be using O-band as well. Therefore, we choose this transmission window for our experiment. Our goal was to push the bit rate using low-bandwidth components within the realm of IM-DD systems. Based on our tests we found that DB-PAM-8 can meet our target with less intensive DSP, and hence, this format was chosen. To tackle the combined effect of ISI and nonlinearity, we have used a Volterra equalizer at the receiver. We report 108, 102, and 84 Gb/s DB-PAM-8 transmission in B2B, and over 10 and 20 km of SMF, respectively. We also obtained receiver sensitivities of -11.5, -9, and -7 dBm for 51, 75 and 99 Gb/s DB-PAM-8 transmission, respectively, in B2B.

Our experimental findings are accompanied by a theoretical framework aimed to calculate the BER of DB-PAM-M signals following an alternative approach to typical error counting. This statistical approach, widely accepted in the calculation of BER for PAM-2 signals [28], [29], is particularly useful to estimate very low BER values corresponding to optical systems that exhibit very good performance (e.g. BER $\leq 10^{-12}$ [30]). Indeed, at such BER values, calculation through error counting becomes impractical due to the long time required. Instead, the approach discussed here avoids the use of extremely long bit sequences. It therefore represents a practical and sufficiently accurate choice, especially when dealing with systems that do not rely in strong forward-error correction. Moreover, due to its simplicity, it has been widely employed for years by waveform measurement instruments to estimate the BER or, equivalently, the quality-factor (Q-factor), from the statistics of the sampled received PAM-2 signal. This is so because, under the assumption of Gaussian distribution of the received noise, correct estimations of these performance metrics can be calculated without having prior knowledge of the launched bit sequence (as it is usually the case while working in the field). This is not the case when calculating the BER or SER (symbol-error rate) through error counting, where the launched bit (symbol) sequence is compared to the received sequence to count the errors; the BER (SER) is then calculated as the ratio of the number of errors to the total number of transmitted bits (symbols). The statistical approach discussed here has also proved to be useful in the approximation of the BER while transmitting PAM-M signals with M = 4, 8 and 16 [5]. In this contribution, we extend the set of equations to the case of duo-binary signals with multiple levels, that is, DB-PAM-M modulation. The accuracy of the approach is verified by comparing against the BER calculated via error counting using the same measured data, obtained with our experimental set up. In particular, it is shown that the proposed formulae for DB-PAM-M match well the corresponding measured BER values, especially as this performance metric exhibits low figures. In other words, for those values where the use of the formalism becomes more practical.

In summary, the main contributions of this work are: 1) The experimental demonstration of a new solution based on partial-response signaling and Volterra nonlinear equalization for high-speed transmission in short-reach optical systems exhibiting relatively narrow bandwidth. 2) An analysis of the performance of this system when varying its bit rate, received optical power and reach, in order to be weighted against other feasible solutions. 3) An analytical model to statistically estimate the BER and SER of DB-PAM-M signals without prior knowledge of the launched bit sequence. The set of equations is particularly useful to calculate very low BER values in a practical manner. 4) The verification of the accuracy of the theoretical framework under different experimental conditions and a study on how this accuracy is related to the correct estimation of the distribution moments. 5) An analysis and explanation of the limitations of the proposed and similar Gaussian models, especially when the eyes are nearly closed (high BER values).

The remainder of the article is organized as follows. Section II presents the experimental testbed used to run the experiments, while Section III provides the experimental results of the DB-PAM-8 transmission. The theoretical approach to calculate the BER for DB-PAM-M signaling is derived in Section IV, followed by extensive experimental verification. Finally, we provide concluding remarks in Section V.

2. Experimental Setup

DB-PAM-8 is a bandwidth-efficient partial response signal, where, controlled inter-symbol interference (ISI) is introduced by strong filtering [19], [22]. The generation method of the DB-PAM-8 signal introduces bit correlation. Hence, the information of former symbols is required for decoding the signal which causes error propagation. To solve this issue, pre-coding is required at the transmitter, which can be done as following [22]:

$$b_k = \mathrm{mod}8(a_k - b_{k-1}) \tag{1}$$

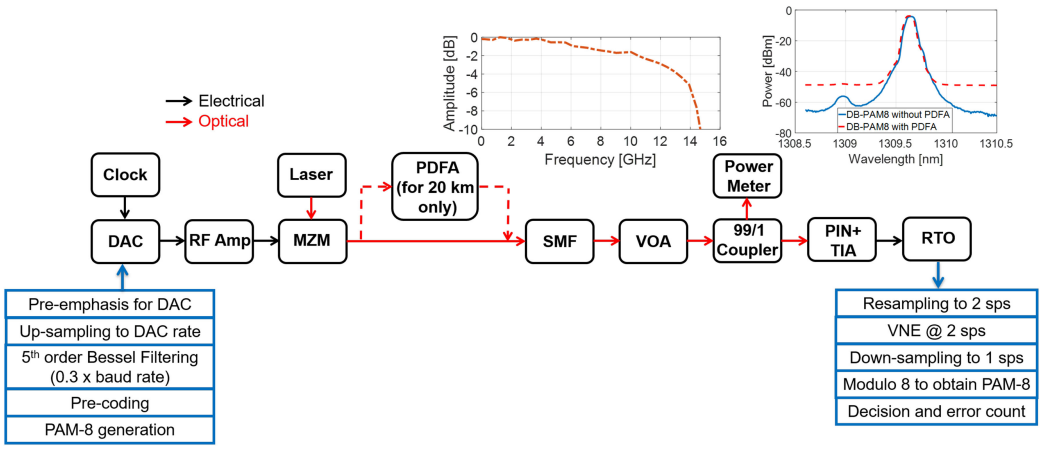

Fig. 1. Experimental testbed, DSP blocks, DB-PAM-8 spectra at 17 GBaud and the system frequency response. DAC: digital-to-analog converter, SMF: single-mode fiber, PDFA: Praseodymium-Doped Fiber Amplifier, MZM: Mach-Zehnder modulator, VOA: Variable optical attenuator, TIA: trans-impedance amplifier, RTO: Real-time oscilloscope.

Here, a_k is the original PAM-8 symbols, and b_k is the pre-coded symbols. The 15-level signal, c_k is generated due to the low-pass filtering of the pre-coded symbols using a 5th order Bessel filter with a cut-off frequency of 0.3 $\times$ baud rate [22]. At the receiver, the PAM-8 symbols are recovered using the following [22]:

$$a_k = \text{mod}8(c_k) \tag{2}$$

The experimental testbed is shown in Fig. 1. The DB-PAM-8 signal is generated using an 8-bit digital-to-analog converter (DAC) at a sampling rate of 64 GSa/s. The frequency response of the DAC is compensated using a real-valued finite-impulse-response (FIR) filter. As mentioned in the previous paragraph, pre-coding and low-pass filtering are done at the transmitter.

The output of the DAC is connected to a RF amplifier having a 3-dB bandwidth of about 40 GHz. The RF amplifier drives an O-band silicon MZM [5] with a 3-dB bandwidth of 20 GHz. The modulator has an optical loss of 4.6 dB at 4 V bias voltage, and 9 dB of coupling loss due to the grating couplers [5]. Thus, the total insertion loss of the modulator is 13.6 dB. A distributed feedback (DFB) laser with an emission wavelength of 1309.7 nm is used as the CW source. The laser is operated at 120 mA current and 20 °C temperature. A praseodymium-doped fiber amplifier (PDFA) having a noise figure of about 7 dB is used after the silicon MZM only for the 20 km fiber case to compensate for the propagation loss so that the signal can be detected using the PIN+TIA (40 GHz 3-dB bandwidth). The PDFA is not required for the B2B and 10 km cases, since the received optical power at the PIN+TIA is within the sensitivity limit. It should be noted that the PDFA would not be required for even 20 km case if the total insertion loss of the silicon MZM (13.6 dB) was smaller and comparable to commercial lithium niobate MZMs (about 3 to 4 dB of insertion loss). The amplification was not done before the silicon MZM since the laser output power is high and it would saturate the PDFA. The signal is propagated over different lengths of standard SMF. After that, the signal is attenuated using a variable optical attenuator (VOA) to sweep the received optical power, followed by a 99/1 coupler to facilitate the received optical power measurements. The signal is detected using a PIN photodetector (PD) with TIA. The detected signal is then digitized using a real-time oscilloscope (RTO) with a sampling speed of 80 GSa/s for offline processing. The bandwidth on the RTO was set at 17 GHz with a 'brick-wall' profile (no information beyond 17 GHz will be received). We have used a third-order Volterra equalizer running at 2 samples/symbol at the receiver before thresholding. The memory length of the three orders are 109, 13, and 3, respectively (found to be optimum after sweeping). The PAM-8 symbols

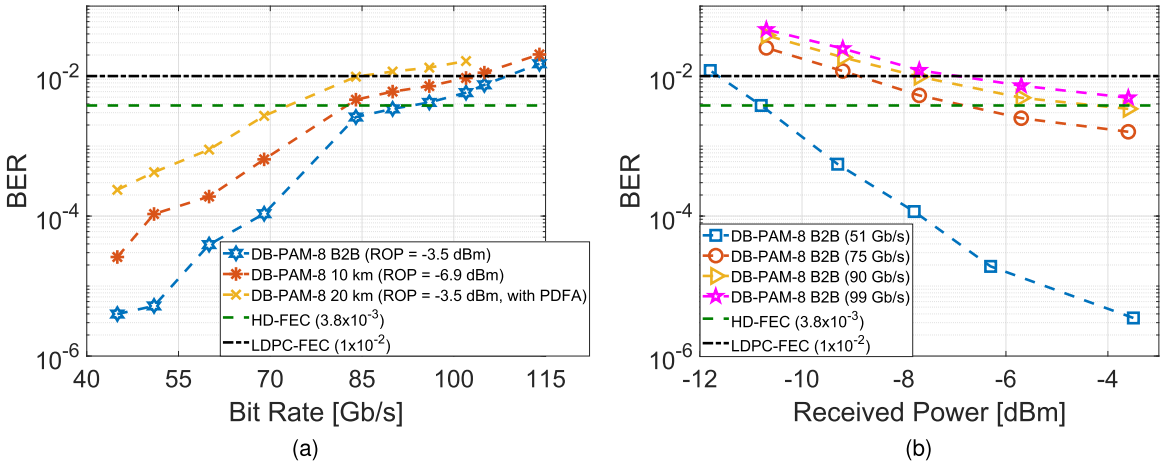

Fig. 2. (a) BER vs bit rate for different reach, and (b) BER as a function of the received optical power at different bit rates in B2B.

are recovered from the 15-level DB-PAM-8 signal using the modulo-8 operation. After clock and data recovery, the BER is calculated from the comparison of the received and the transmitted bit sequences. The frequency response of the overall system excluding the SMF is shown in Fig. 1, which exhibit 12 GHz of 3-dB system bandwidth. The DSP blocks at the transmitter and receiver, and the DB-PAM-8 spectra are shown as well in Fig. 1.

3. Experimental Results

In this section, we present the BER performance of the DB-PAM-8 transmission. We vary the bit rate, reach and received optical power, and report the BER as functions of these performance parameters. Figure 2(a) shows the BER performance for different bit rates and reach. We also provide two different FEC thresholds including hard-decision FEC (HD-FEC) (3.8×10^{-3}, 7% overhead) and LDPC-FEC (1×10^{-2}, 17% overhead) [31] for reference purpose. Bit rates of 108, 103, and 85 Gb/s are achieved below the LDPC-FEC threshold, and 93, 83, and 73 Gb/s are achieved below the HD-FEC threshold in B2B, and after 10 and 20 km propagation, respectively. Although we are operating at a wavelength close to the zero dispersion wavelength of the SMF, significant performance difference can be observed in the 10 and 20 km cases compared to B2B. The received optical powers are -3.5 dBm for the B2B case and -6.9 dBm for the 10 km propagation case. Hence, there is a penalty in terms of BER for the 10 km case due to lower received optical power (ROP) rather than due to the influence of fiber chromatic dispersion. The BER performance of these two and other ROP values at different bit rates can be observed for the B2B situation in Fig. 2(b). A more pronounced slope is evident at lower bit rates. This agrees with the higher BER difference observed between the B2B and 10-km curves in Fig. 2(a) at those bit rates. As mentioned before, due to the high propagation loss in the O-band, we had to amplify the signal using a PDFA for the 20 km case. Following this approach, we kept the ROP within the detection limits of the PIN+TIA and maintained it at -3.5 dBm at the input of the receiver. Therefore, the penalty for the 20 km case can be attributed in part to the noise added by the PDFA (since we did not use an optical band-pass filter to remove the out-of-band noise after amplification), but mainly to the difficulty faced by the Volterra equalizer to differentiate between the fifteen levels in a relatively (with respect to the B2B case) closed eye. Despite that the Volterra equalizer works better when the noise level in the eye is lower, it still carries out a significant performance improvement. This can be confirmed when comparing the DB-PAM-8 curve of Fig. 2(a) for B2B with that presented

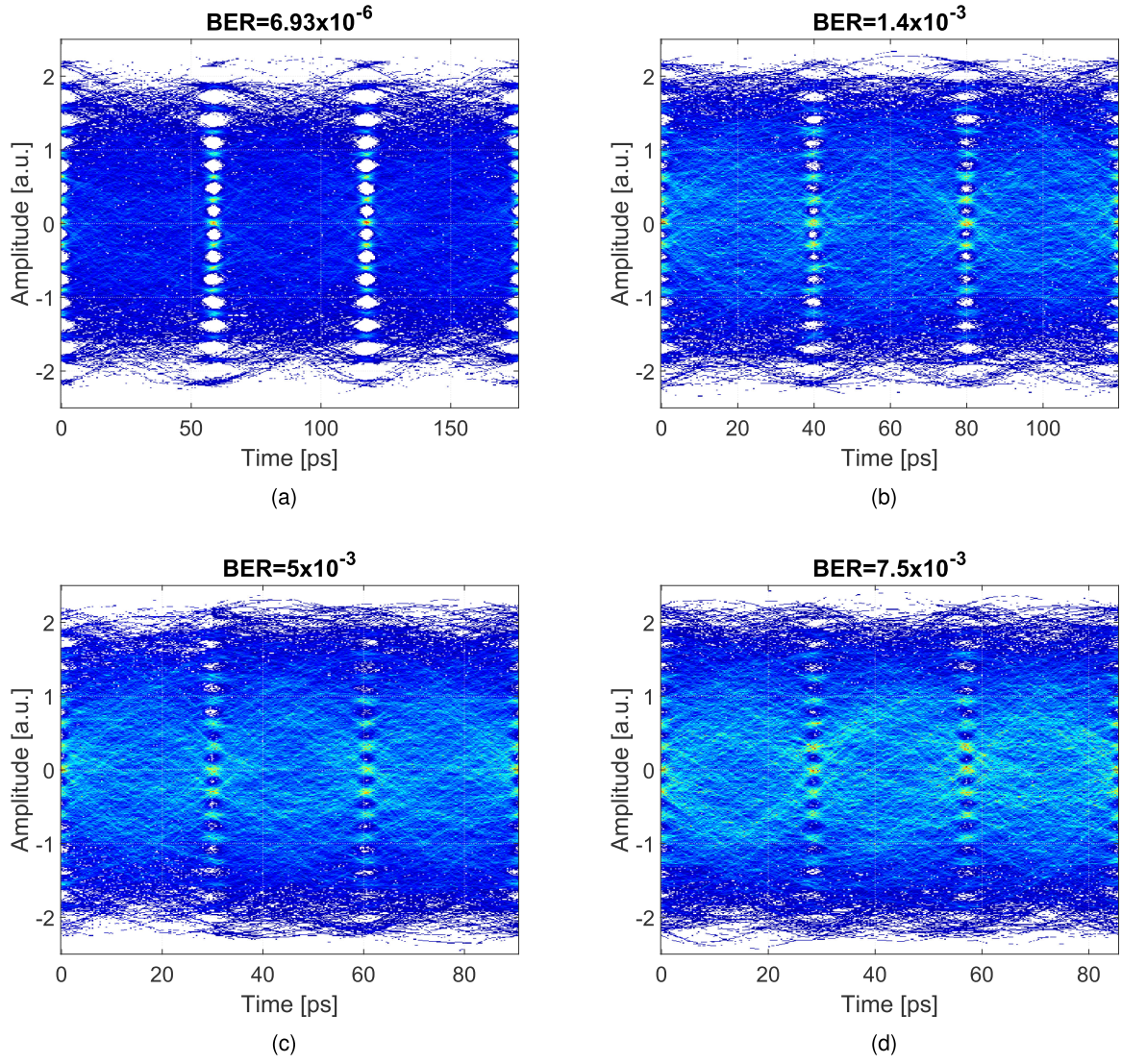

Fig. 3. DB-PAM-8 eye diagrams at (a) 51 Gb/s (17 GBaud), (b) 75 Gb/s (25 GBaud), (c) 99 Gb/s (33 GBaud), and (d) 105 Gb/s (35 GBaud) in B2B.

in Fig. 5(a), whose BER values were obtained from the same received signals but processed using a linear Volterra filter, as discussed below.

The BER as a function of the ROP is presented in Fig. 2(b) for different bit rates. Receiver sensitivities of -11.5, -9, -8 and -7 dBm are obtained below the LDPC-FEC threshold for bit rates of 51, 75, 90 and 99 Gb/s, respectively, and -11, -7 and -4 dBm are achieved below the HD-FEC threshold for bit rates of 51, 75 and 90 Gb/s, respectively. The BER is slightly above HD-FEC threshold for the 99 Gb/s transmission case. The eye diagrams of the DB-PAM-8 signals for different bit rates in B2B configuration are shown in Fig. 3. The 15-level DB-PAM-8 signal can be clearly distinguished in all diagrams.

TABLE I

A Priori Probabilities of Equation (3) for DB-PAM-M Modulation, Derived Using Equation (4)

M=2							$\frac{1}{4}$	$\frac{2}{4}$	$\frac{1}{4}$							
M=4					$\frac{1}{16}$	$\frac{2}{16}$	$\frac{3}{16}$	$\frac{4}{16}$	$\frac{3}{16}$	$\frac{2}{16}$	$\frac{1}{16}$					
M=8	$\frac{1}{64}$	$\frac{2}{64}$	$\frac{3}{64}$	$\frac{4}{64}$	$\frac{5}{64}$	$\frac{6}{64}$	$\frac{7}{64}$	$\frac{8}{64}$	$\frac{7}{64}$	$\frac{6}{64}$	$\frac{5}{64}$	$\frac{4}{64}$	$\frac{3}{64}$	$\frac{2}{64}$	$\frac{1}{64}$	

4. BER Modeling of DB-PAM-M Modulation Formats

Let $[a_n] \in \{0, 1, \ldots, i, \ldots, M-1\}$ be a PAM-M data stream of n symbols. After precoding following (1) and adequate filtering, $[a_n]$ becomes $[c_n] \in \{0, 1, \ldots, i, \ldots, 2M-2\}$, the corresponding duo-binary PAM-M data stream of $2M-1$ levels. Following (2), $[a_n]$ can be recovered from its duo-binary counterpart as $[a_n] = mod M([c_n])$. Transmission of $[c_n]$ through the optical channel is accomplished by mapping (using a DAC) its symbols to the $2M-1$ levels of an electrical signal, which in turn drives an optical modulator. After fiber propagation, detection, adequate clock-recovery and processing, the received electrical duo-binary signal is sampled at the time corresponding to approximately the borderline between symbols (rather than in the midpoint of the symbol time slot), that is, 30.3 ps in a DB-PAM-8 signal of 99 Gb/s (see, e.g., Fig. 3(c)). It is then sliced using $2M-2$ thresholds, resulting in data stream $[c'_n]$. The SER can then be calculated through error counting, as already explained, by comparing $[a_n]$ to $[a'_n] = mod M([c'_n])$. Under the assumption of Gray coding, the BER can be calculated as $BER = SER/(log_2 M)$. It corresponds to the minimum BER case, where only one bit of the symbol is erroneous. If this is not the actual situation, then $SER \geq BER \geq SER/(log_2 M)$. Throughout this paper we will assume the minimum BER case.

An alternative approach to calculate the BER (or SER) of DB-PAM-M signals is to determine the statistics of the amplitude fluctuations of the electrical signal (normally the voltage) that corresponds to each amplitude level l_i after sampling and slicing [28]. By associating the error probability to the SER, the latter can be calculated from the aforementioned statistics using the total probability theorem [32] as:

$$SER_Q = \sum_{i=0}^{2M-2} p(l_i) \left(P(l_{i-1}|l_i) + P(l_{i+1}|l_i) \right) ; \tag{3}$$

where $P(l_{i+1}|l_i)$ is the conditional probability of deciding that one of the symbols corresponding to levels l_{i+1}, l_{i+2}, …, l_{2M-2} was received when the symbol corresponding to level l_i was actually transmitted; that is, making a decision mistake. Similarly, $P(l_{i-1}|l_i)$ is the conditional probability of deciding that one of the symbols corresponding to levels l_{i-1}, l_{i-2}, …, l_0 was received when the symbol corresponding to level l_i was actually transmitted. Note that $P(l_{-1}|l_0) = P(l_{2M-1}|l_{2M-2}) = 0$ because l_{-1} and l_{2M-1} do not correspond to signal levels and hence there is no possible error. We have appended subscript Q to the statistically calculated SER (BER) to distinguish it from the SER_{EC} (BER_{EC}) calculated via error counting. The subscript remind us that the Q-factor can be derived from the BER_Q as Q-factor $= \sqrt{2}\,\text{erfcinv}(2BER_Q)$ [28], where (erfcinv) erfc is the (inverse of) the complementary error function. In (3), $p(l_i)$ represents the a priori probability of level i. For PAM-M signaling a similar formula holds [5], but since in this case all amplitude levels are equally likely to occur, $p(l_i) = 1/M, \forall i$. The situation is different in DB-PAM-M, where the a priori probabilities are calculated with the following formula that can be derived by algebraic or numerical methods. Here we assume, as it is usually the case, a uniform a priori probability distribution for the M PAM-M levels that turn into the corresponding $2M-1$ duo-binary levels after adequate filtering:

$$p(l_i) = \frac{M - |i - (M-1)|}{M^2}; \; i = 0, 1, \ldots, 2M-2. \tag{4}$$

Table 1 shows the a priori probabilities for some values of M.

In contrast to PAM-M, where each amplitude level transport approximately the same amount of symbols, the shape of the overall probability density function for the adequately sampled DB-PAM-M signal, $\sum_{i=0}^{2M-2} f(l_i)$, where $f(l_i)$ stands for the probability density function of level l_i, is rather

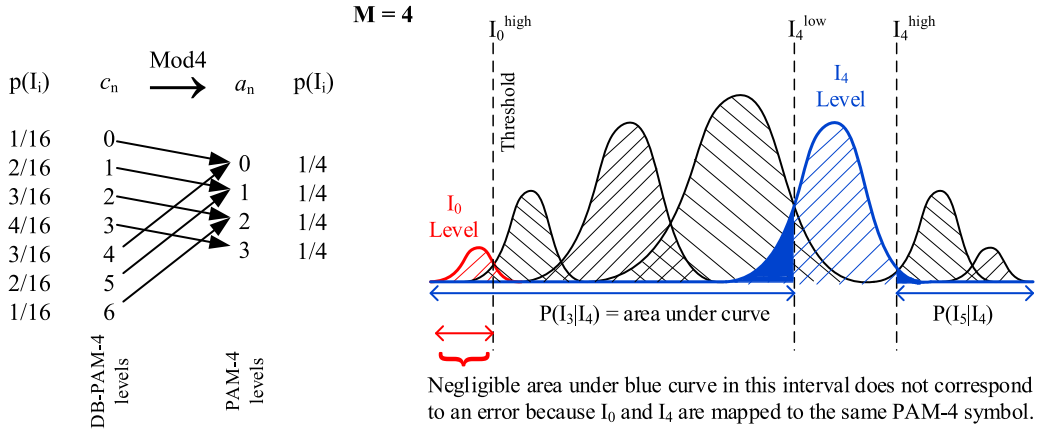

Fig. 4. Mapping between DB-PAM-4 and PAM-4 levels via *mod*4 operation and graphical illustration of the conditional probability of error of level l_4, which is the area under the Gaussian curve (solid blue) calculated out of the (l_4^{low}, l_4^{high}) interval.

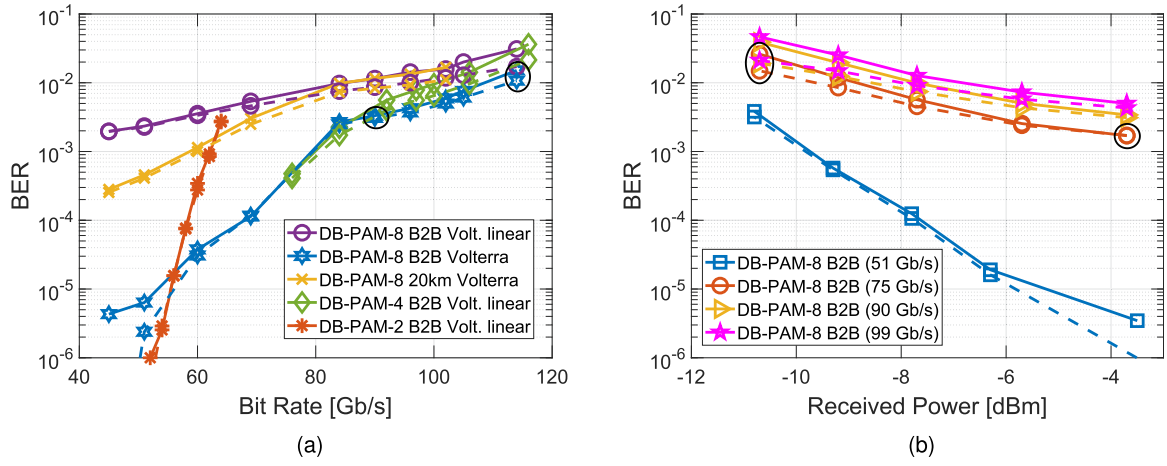

Fig. 5. (a) BER as a function of bit rate for M = 2, 4 and 8, and (b) BER as a function of the received optical power at different bit rates in B2B. Solid (dashed) curves correspond to BER_{EC} (BER_Q). The circles indicate the points corresponding to the histograms of Fig. 6.

triangular (see Fig. 6). This is not the case in the overall probability density function of PAM-M (see, e.g., Fig. 11 of [5]), which is approximately uniform. Therefore, the outer amplitude levels of the DB-PAM-M signal transport less symbols than the central level and consequently, the nonlinear characteristics of the transfer function of the MZM and photodiode, which mainly affects the outer and higher levels, respectively, have a lower impact than in the PAM-M case. Of course, the total number of symbols (and bits) transported by the PAM and the DB-PAM signals during a given period of time is the same. It is only the way in which the corresponding symbols are distributed along the amplitude levels (and, of course, the number of levels) in both modulation formats that is different. For instance, let M = 4. For transforming the DB-PAM-4 signal $[c_n]$, having 7 levels, into the PAM-4 signal $[a_n]$, having 4 levels, the following equation is used: $[a_n] = mod4([c_n])$. This means that the symbol count of level 6 of the DB-PAM-4 signal will be added to level 2, because, once transformed to PAM-4, both levels represent the same PAM-4 symbol from the alphabet. That is, $mod4(6) = 2$. Let us remind the reader at this point that at the very input/output of the system we

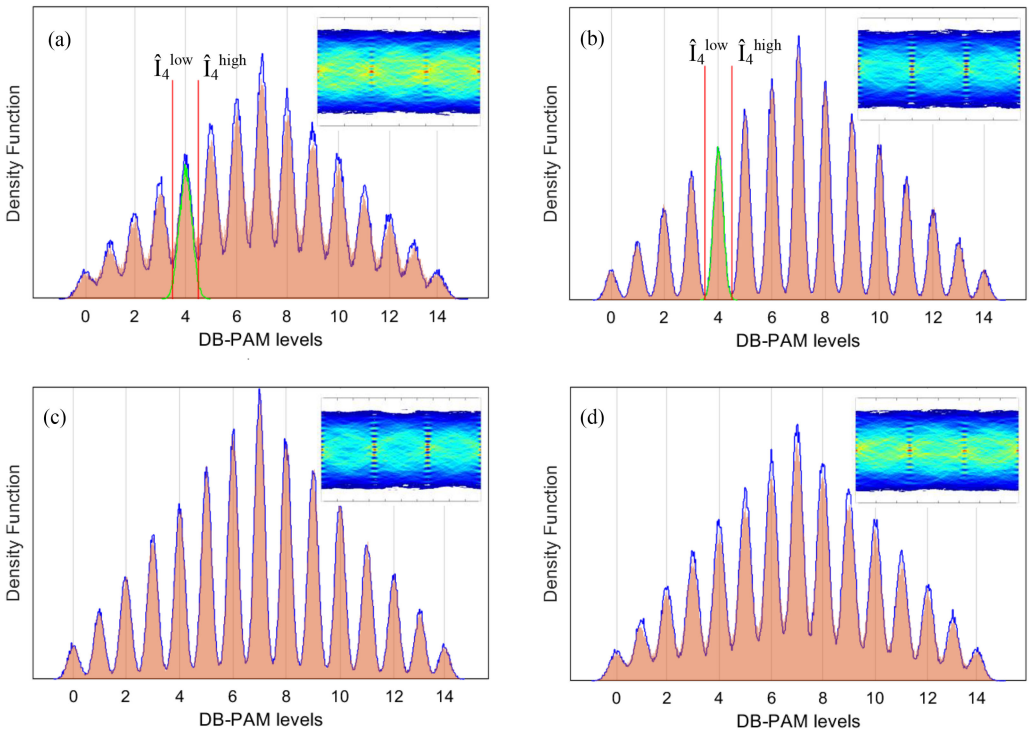

Fig. 6. Histograms of the B2B DB-PAM-8 received signal samples (orange) and corresponding fit using Gaussian density functions (blue line). ROP values of −10.7 (a) and −3.7 (b) dBm for a bit rate of 75 Gb/s. Bit rates of 90 (c) and 114 (d) Gb/s. The corresponding points in Fig. 5 are marked with circles. The insets show the respective eye diagrams.

are dealing with a PAM-M signal. Similarly, level 5 will be added to level 1 ($mod4(5) = 1$), and level 4 will be added to level 0. Following this reasoning, the a priori probabilities of DB-PAM-4 should also add up to the corresponding a priori probabilities of PAM-4 once transformed back from DB-PAM-4 signaling. In other words, the a priori probabilities of levels 6 (1/16) and 2 (3/16) of the DB-PAM-4 signal add up to 1/4, the a priori probability of level 2 of the PAM-4 signal. In a similar manner, the a priori probabilities of levels 5 (2/16) and 1 (2/16) of the DB-PAM-4 signal also add up to 1/4, the a priori probability of level 1 of the PAM-4 signal. The same occurs with levels 4 and 0. This phenomenon is illustrated in the left hand side of Fig. 4 that shows how the DB-PAM-4 levels (and corresponding probabilities) are mapped onto the PAM-4 levels via the *mod*4 operation. Of course, in both modulation formats, DB-PAM-4 and PAM-4, the sum of $p(I_i)\ \forall i$ is one. Note that 3 is the only level having a one to one correspondence between the elements of $[a_n]$ and $[c_n]$, whereas for the rest of the levels, two elements of $[c_n]$ are mapped onto $[a_n]$. The generalization to M levels is straightforward.

Assuming Gaussian statistics for the fluctuations in each amplitude level, the corresponding probability density functions become $f(I_i) = \frac{1}{\sigma_i\sqrt{2\pi}} \exp(\frac{(I_i-\mu_i)^2}{-2\sigma_i^2})$, and considering the minimum BER case, equation (3) becomes:

$$BER_Q = \frac{1}{2\log_2 M} \sum_{i=0}^{2M-2} p(I_i) \left[\text{erfc}\left(\frac{\mu_i - I_i^{\text{low}}}{\sqrt{2}\sigma_i} \right) + \text{erfc}\left(\frac{I_i^{\text{high}} - \mu_i}{\sqrt{2}\sigma_i} \right) \right]; \tag{5}$$

where μ_i is the estimated average value of the received symbols that were transmitted as I_i, and σ_i^2 is their estimated variance.

The quantities I_i^{low} and I_i^{high} are the optimum decision level thresholds between I_{i-1} and I_i, and between I_i and I_{i+1}, respectively. Note that since I_{-1} and I_{2M-1} do not correspond to signal levels, $I_0^{low} \to -\infty$ and $I_{2M-2}^{high} \to \infty$, and hence $erfc(\frac{\mu_0 - I_0^{low}}{\sqrt{2}\sigma_0}) = erfc(\frac{I_{2M-2}^{high} - \mu_{2M-2}}{\sqrt{2}\sigma_{2M-2}}) = 0$. Fig. 4 graphically illustrates, for M = 4, the conditional probability of error of level I_4, that is, $P(I_3|I_4) + P(I_5|I_4)$. It consists of the integral (area under the blue curve) of $f(I_4)$ from $-\infty$ to ∞, except from the interval (I_4^{low}, I_4^{high}), which corresponds to a correct decision. This can be expressed as $\int_{-\infty}^{I_4^{low}} f(I_4)dI + \int_{I_4^{high}}^{\infty} f(I_4)dI$. It is highlighted in solid blue in Fig. 4. It must be noted, however, that formally, equation (5) is only an approximation. This comes from the fact that two levels of the DB-PAM-M sequence $[c_n]$ are mapped onto the same level of the PAM-M sequence $[a_n]$ as illustrated in the left hand side of Fig. 4 for M = 4; that is, two DB-PAM-M levels account for the same PAM-M symbol (except for the central level, whose a priori probability is 1/M). Consequently, a probability of error term corresponding to the complementary level should in principle be subtracted from each term of the summation (except for $i = M$) in equation (5). For example, for M = 4, the complementary level of I_4 is $I_0 = I_{mod4(4)}$ and vice versa. Then, according to Fig. 4, the integral (area under the blue curve) of $f(I_4)$, spanning from $-\infty$ to I_0^{high} (the interval is marked with red in Fig. 4) should be substracted from $\int_{-\infty}^{I_4^{low}} f(I_4)dI$ because actually the integral calculated on this interval does not correspond to an error. In the same manner, $\int_{I_4^{low}}^{I_4^{high}} f(I_0)dI$ should in principle be substracted from $P(I_1|I_0)$. In practice, however, due to the fact that the complementary levels are M levels apart from each other and that the density functions $f(I_i)$ are tightly concentrated around μ_i, the aforementioned probability terms that have to be subtracted can be neglected without affecting the actual BER outcome, as experimentally shown below. Even from Fig. 4, it is graphically evident that the terms being discussed are practically negligible.

The use of Gaussian statistics is convenient because the mathematical problem becomes tractable and the amplitude fluctuations around μ_i become characterized by a single parameter σ_i^2 that contains all sources of noise accumulated along the optical path, together with the photodiode noise. In particular, it includes the signal-ASE beat noise, the ASE-ASE beat noise, the thermal noise and the shot noise. The two latter sources, produced by the photodiode, can be approximated with Gaussian statistics. The accuracy of our formalism will increase as the random variables that characterize the noise sources and the density function of their sum become closer to Gaussian. In other words, when the noise produced by the optical receiver, as opposed to optical noise, dominates. We expect this to be actually the case in our measurements, especially in the unamplified situation. Assuming that most of the errors are caused by the amplitude fluctuations exhibited by neighboring levels, the optimum threshold values can be calculated through a generalization to $2M - 1$ levels of the 2-level equation presented in Eq. (2) of Ref. [5], as:

$$I_i^{low} = \frac{\mu_{i-1}\sigma_i^2 - \mu_i\sigma_{i-1}^2 + \sigma_i\sigma_{i-1}\sqrt{(\mu_i - \mu_{i-1})^2 + 2(\sigma_i^2 - \sigma_{i-1}^2)\ln(\sigma_i/\sigma_{i-1})}}{\sigma_i^2 - \sigma_{i-i}^2}, \tag{6}$$

$$I_i^{high} = \frac{\mu_i\sigma_{i+1}^2 - \mu_{i+1}\sigma_i^2 + \sigma_{i+1}\sigma_i\sqrt{(\mu_{i+1} - \mu_i)^2 + 2(\sigma_{i+1}^2 - \sigma_i^2)\ln(\sigma_{i+1}/\sigma_i)}}{\sigma_{i+1}^2 - \sigma_i^2}. \tag{7}$$

To test the accuracy of BER_Q (Eq. (5)) against BER_{EC} (error counting), we calculated the value of both metrics using exactly the same data measured with the experimental setup described in Section II. Similar to Fig. 2, the analysis was carried out by varying the bit rate and the received optical power of the transmitted signal. The corresponding graphs are shown in Fig. 5, where the solid curves correspond to BER_{EC} (the reference) and the dashed curves correspond to BER_Q (the model). We also extended the investigation to consider M = 2 and M = 4. The corresponding signals were experimentally produced with a setup similar to that described in Section II and under similar conditions. In Fig. 5(a), the DB-PAM-8 curves for B2B (blue with stars) and 20-km propagation (yellow with x) correspond to those shown in Fig. 2(a). For the sake of comparison, we have also included the DB-PAM-8 BER values in B2B configuration, but calculated using a

first-order Volterra equalizer having a memory length of M1 = 32 (purple curve with circles). This graph demonstrates the favorable impact of using the Volterra equalizer to improve the system performance of the DB-PAM-8 signal. The same linear Volterra equalizer was used to generate the BER curves for DB-PAM-4 (green with diamonds) and DB-PAM-2 (orange with asterisks) signaling. The improvement provided by the nonlinear Volterra filter in the M = 2 and M = 4 cases was rather marginal and hence we opted for the, less complex, linear processing algorithm. The solid curves presented in Fig. 5(b) correspond to those shown in Fig. 2(b), while the dashed curves were obtained using the Gaussian model here put forward.

The curves in Fig. 5 indicate that, in general, equation (5) represents a good model to calculate the BER of a transmission system when using DB-PAM-M modulation, even after Volterra equalization, especially as the BER values become low. As mentioned before, these are also the circumstances under which the Gaussian model becomes more necessary and useful because, as the DB-PAM-8 curves for the B2B case demonstrate, the (necessarily) limited number of bits employed for the calculation of BER_{EC} sets a minimum level below which we cannot report BER_{EC} with sufficient confidence. In our case this level is around 10^{-5} because we launched 2^{20} bits into our system (since $12/2^{20} \approx 1.1 \times 10^{-5}$, we are actually considering a safety margin of 12 mistakes –or 4 symbols– while counting the erroneous bits) [33]. Hence, the use of equation (5) represents a more sensible choice when estimating the BER below this bound. This also explains the discrepancy between BER_{EC} and BER_Q observed in Fig. 5(a) for the B2B DB-PAM-8 (blue) curve at bit rates of 45 and 51 Gb/s and in the corresponding curve of Fig. 5(b) for a ROP of -3.7 dBm and a bit rate of 51 Gb/s. At these points, BER_{EC} is providing inaccurate results.

The curves in Fig. 5 also show that the Gaussian model exhibits a prevailing system performance overestimation, whose degree varies according to system conditions such as bit rate and ROP. These observations make it clear that, although the assumption of Gaussian density functions for $f(l_i)$ is accurate enough, there still exists a natural deviation between the measured and the calculated curves. According to Figs. 5(a) and 5(b) this deviation increases as the calculated BER values become higher than approximately 5×10^{-3}, thus resulting in an increasing difference between the BER_{EC} (solid) and BER_Q (dashed) curves. To understand why the Gaussian model becomes inaccurate when dealing with very high BER values, we resort to Fig. 6 that depicts the histogram of the received signal samples (orange background) and the corresponding fit (blue line) assuming a Gaussian density function for each amplitude level. The respective eye diagrams are also shown in the insets. Figs. 6(a) and 6(b), were obtained from the DB-PAM-8 B2B system running at 75 Gb/s, with received signals having a ROP of -10.7 and -3.7 dBm, respectively. Similarly, Figs. 6(c) and 6(d), were obtained from the DB-PAM-8 B2B system running at 90 and 114 Gb/s, respectively. The corresponding points in Fig. 5 are marked with black circles.

In order to calculate BER_Q via equation (5), μ_i and σ_i^2 have to be calculated for each amplitude level, l_i. They characterize the assumed Gaussian density functions (blue curves in Fig. 6). We calculated the mean and variance by applying well-known unbiased estimators [32] to the observation vector $\vec{x_i} = (x_1^i, x_2^i, \ldots, x_k^i)$, $i = 0, \ldots, 2M-2$, consisting of the k received signal samples pertaining to each of the 2M-1 levels that are obtained after slicing using optimum decision thresholds. The mean and variance for each level can be written as: $\mu_i = \frac{1}{k}\sum_{j=1}^{k} x_j^i$ and $\sigma_i^2 = \frac{1}{k-1}\sum_{j=1}^{k}(x_j^i - \mu_i)^2$ [32]. In situations where the histogram of the received samples resembles that shown in Fig. 6(b), that is, in situations where the general noise level and amplitude fluctuations around μ_i are low, the eyes are sufficiently open and the Gaussian density function of each level can be clearly distinguished from those of its neighbor functions, then vector $\vec{x_i}$, obtained after the slicing process, incorporates most of the samples corresponding to the actual function $f(l_i) = \frac{1}{\sigma_i\sqrt{2\pi}}\exp(\frac{(l_i-\mu_i)^2}{-2\sigma_i^2})$. This is illustrated in Fig. 6(b) for $f(l_4)$ (in green). Since the width of each density function is narrow enough as compared to $|\mu_i - \mu_{i\pm1}|$, the slicing process that employs optimum decision thresholds, $\hat{l}_4^{low}$ and $\hat{l}_4^{high}$ (in red), only leaves a few samples of $f(l_4)$ out of the slicing interval ($\hat{l}_4^{low}$, $\hat{l}_4^{high}$). The calculation of σ_i^2 becomes accurate enough and therefore the sum of the calculated Gaussian density functions (blue curve) closely matches the histogram of the received signal samples (orange background). Consequently, BER_{EC} and BER_Q coincide. In contrast, in situations where one finds large amplitude

fluctuations around μ_i that are produced by the limited opto-electronic bandwidth of the system, or when there are noise sources present in the received signal, such as ASE-ASE and ASE-signal beat noise, and especially, thermal and shot–noise (whose statistics are intrinsically Gaussian), there is a spreading of the amplitude (normally the voltage) pertaining to level l_i to adjacent neighbor levels. The eyes then become partially closed and the Gaussian density function of each level cannot longer be clearly distinguished from those characterizing neighbor levels. This is the situation observed in Fig. 6(a), where an electrical signal with low SNR (consequence of a low power optical signal impinging into an optical receiver exhibiting comparatively powerful noise sources) is analyzed. Here, the typical slicing process using optimum decision thresholds $\hat{l}_4^{\text{low}}$ and $\hat{l}_4^{\text{high}}$ (in red) leaves a considerable amount of samples pertaining to the actual $f(l_4)$ (in green) outside the slicing interval $(\hat{l}_4^{\text{low}}, \hat{l}_4^{\text{high}})$. The samples in vector $\vec{x}_i$ will then be insufficient for an accurate estimation of σ_i^2 (dependent on $(x_j^i - \mu_i)^2$), which in general will be underestimated, and hence the sum of the calculated Gaussian density functions (blue curve) will not accurately match the histogram of the received signal samples (orange background). Too narrow Gaussians (in blue) are observed for the fits in Fig. 6(a), leading to the consequent disagreement between BER_{EC} and BER_Q and the corresponding mismatch of the curves in Fig. 5(b) for low ROP values. The aforementioned arguments also apply to Figs. 6(c) and (d). In this case, however, the large amplitude fluctuations observed in the histogram (and corresponding eye closure) of Fig. 6(d) for high bit rates, are a consequence of the limited opto-electronic system bandwidth rather than the presence of noise induced by the photo-detection process itself.

From the discussion, it can then be concluded that the disagreement between BER_{EC} and BER_Q observed in Fig. 5 at high BER values cannot be ascribed to the fact of having chosen Gaussian statistics to approximate the amplitude fluctuations found around each level, but rather to the procedure employed to slice the sampled signal under these unfavorable conditions (of Gaussian overlapping and relative eye closure). Samples slicing through the use of optimum decision thresholds, nonetheless, is common practice in IM/DD systems. We have also investigated other techniques to capture all the required samples obtained after thresholding with the aim of properly estimating σ_i^2 when the noise of each transmission level is high or the amplitude levels are too close to each other, but we have been unsuccessful. Proper estimation of σ_i^2 can be achieved, nonetheless, when one has prior knowledge of the launched bit sequence. Although such an alternative procedure to calculate σ_i^2 exhibits low pragmatic value, it is useful to substantiate our conclusion. Indeed, if the launched bit sequence is known, slicing after clock-recovery takes place by selecting the samples pertaining to each amplitude level, irrespective of how far they are from μ_i, and without utilizing any threshold. Then, the observation vector $\vec{x}_i$ will contain all the samples necessary to properly calculate σ_i^2. In spite of any Gaussian function overlap, the estimation of σ_i^2 will now be correct because vector $\vec{x}_i$ contains all the samples pertaining to $f(l_i)$ (e.g., green curve in Fig. 6), instead of those pertaining to a severed version of $f(l_i)$, obtained via thresholding. This can be demonstrated in Fig. 7, that shows the same curves of BER_{EC} presented in Fig. 5 (solid lines) as well as the corresponding ones calculated with (5) where σ_i^2 has been estimated by means of the aforementioned procedure (dotted curves; we have used different size and color for the marks for the ease of distinction). The match between solid and dotted curves is now excellent, thus confirming the Gaussian nature of the amplitude fluctuations and the accuracy of our model. Of course, for the analysis of most practical situations in optical transmission systems, where the Gaussian density functions do not overlap (i.e., the eye diagrams are sufficiently open), either method to estimate σ_i^2, and hence BER_Q, will lead to the same result.

It is interesting to note that, in general, there is a better match between BER_{EC} and BER_Q for the DB-PAM-M case (presented here) as compared to the (non-DB) PAM-M case (presented in [5], see Fig. 13). The divergence between both metrics for the PAM-M case is explained by Chagnon *et al.* through two main tenets: 1) the nonlinear behavior of the transmission function of the transmitter affects the outer levels of PAM-M signals, and 2) the PIN + TIA receiver saturates when receiving the highest PAM level of a high power signal. Both effects modify the additive white Gaussian noise assumption employed in the BER_Q calculation [5]. None of both explanations, however, strictly

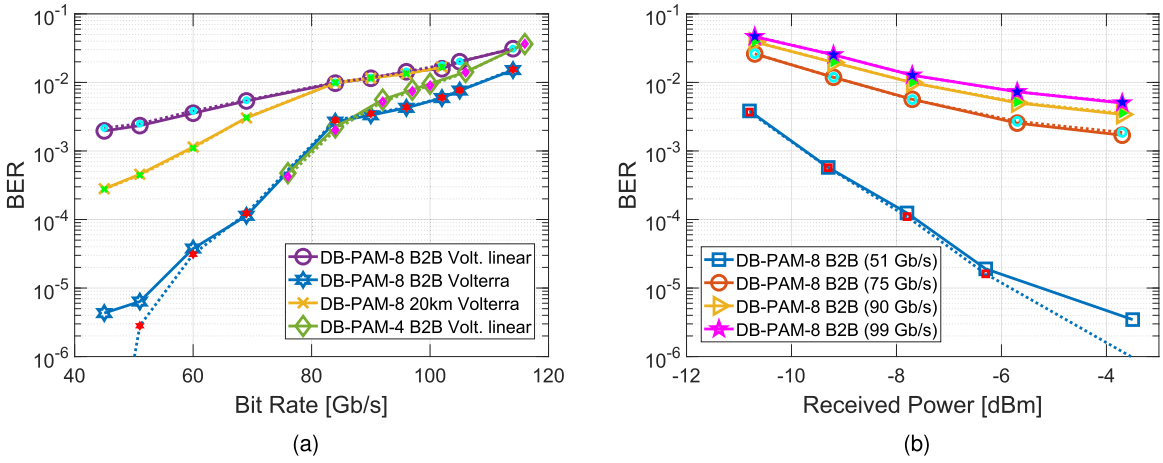

Fig. 7. (a) BER as a function of bit rate, and (b) BER as a function of the received optical power at different bit rates in B2B. Solid curves correspond to BER_{EC}, as in Figs. 2 and 5. Dotted curves correspond to BER_Q, where the variance associated to the Gaussian model (Eq. (5)) is accurately estimated. Different size and color for the marks are set for visual aid purposes.

applies to our investigation because DB-PAM-M signaling exhibits a triangular power distribution among amplitude levels. Therefore, the effect of the transmission function nonlinearity of transmitter and receiver in the signal has a milder effect as compared to PAM signaling. This is because in DB-PAM-M a lower number of symbols are transmitted in the outer levels, becoming less affected by the aforementioned nonlinear characteristics. Moreover, during the execution of the experiment, care was taken to keep the swing of the MZM within reasonable limits so as to avoid entering in the nonlinear operation region of the device. This discussion hence validate our analysis (and the one presented in [5], of course) and put forward some of the differences between PAM and DB-PAM signaling in terms of performance and BER modeling.

V. Conclusion

We have experimentally demonstrated 108 Gb/s DB-PAM-8 transmission using a silicon MZM enabled by Volterra equalizer. The BER performance of the system has been studied as a function of the bit rate, reach and received optical power. Up to 108, 102, and 84 Gb/s signal propagation are achieved in B2B, and over 10, and 20 km of standard SMF, respectively, below the LDPC-FEC. A practical model of the BER for DB-PAM-M signals using a statistical approach has been put forward as well. The match between this model (BER_Q) and BER_{EC} has been verified and discussed. The model is particularly accurate where it is more useful, that is, for BER values below 10^{-3}. It then becomes more valuable in the analysis of high-performance (low-BER) optical systems, where the calculation of BER via error counting becomes impractical due to the excessive number of bits required for the calculation. Moreover, the presented model does not require prior knowledge of the transmitted bits to estimate BER. Our research work represents a step forward to foster the use of partial response signaling in photonic systems.

References

[1] A. K. Srivastava, M. Glick, and Y. Akasaka, "Metro and data center optical networks and short-reach links II," in *Proc. SPIE*, vol. 10946, 2019, pp. 1094 60 1–1.
[2] M. G. Saber *et al.*, "Integrated polarisation handling devices," *IET Optoelectron.*, vol. 14, no. 3, pp. 109–119, 2019.

[3] M. G. Saber *et al.*, "Silicon-based optical links using novel direct detection, coherent detection and dual polarization methods for new generation transport architectures," *Opt. Commun.*, vol. 450, pp. 48–60, 2019.
[4] K. Zhong *et al.*, "Experimental study of PAM-4, CAP-16, and DMT for 100 Gb/s short reach optical transmission systems," *Opt. Exp.*, vol. 23, no. 2, pp. 1176–1189, 2015.
[5] M. Chagnon *et al.*, "Experimental study of 112 Gb/s short reach transmission employing PAM formats and SiP intensity modulator at 1.3 μm," *Opt. Exp.*, vol. 22, no. 17, pp. 21018–21036, 2014.
[6] E. El-Fiky *et al.*, "200 Gb/s transmission using a dual-polarization O-band silicon photonic intensity modulator for stokes vector direct detection applications," *Opt. Exp.*, vol. 25, no. 24, pp. 30336–30348, 2017.
[7] J. Lee, P. Dong, N. Kaneda, and Y.-K. Chen, "Discrete multi-tone transmission for short-reach optical connections," in *Proc. Opt. Fiber Commun. Conf.*, 2016, pp. 1–3.
[8] P. Torres-Ferrera, S. O. Vazquez, and R. Gutiérrez-Castrejón, "4 x 100 Gb/s WDM DD-OFDM using EAM for next generation Ethernet transceivers over SMF," *Opt. Commun.*, vol. 365, pp. 86–92, 2016.
[9] A. Gatto, M. Rapisarda, P. Parolari, and P. Boffi, "Discrete multitone modulation for short-reach mode division multiplexing transmission," *J. Lightwave Technol.*, vol. 37, no. 20, pp. 5185–5192, 2019.
[10] M. I. Olmedo *et al.*, "Multiband carrierless amplitude phase modulation for high capacity optical data links," *J. Lightw. Technol.*, vol. 32, no. 4, pp. 798–804, 2013.
[11] M. Che, T. Kuboki, and K. Kato, "Nonlinear compensation for indoor visible light communication systems with carrierless amplitude and phase modulation," *Japanese J. Appl. Phys.*, vol. 58, no. SJ, 2019, Art. no. SJJA02.
[12] M. G. Saber *et al.*, "Demonstration of a 120 hybrid based simplified coherent receiver on SOI for high speed PON applications," *Opt. Exp.*, vol. 26, no. 24, pp. 31222–31232, 2018.
[13] C. Yang, W. Li, and S. Yu, "Single channel 224 Gb/s (56-GBaud) PAM-16 transmission using linear digital pre-distortion," *Electron. Lett.*, vol. 53, no. 21, pp. 1420–1422, 2017.
[14] M. G. Saber *et al.*, "25 and 50 Gb/s/λ PAM-4 transmission over 43 and 21 km using a simplified coherent receiver on SOI," *IEEE Photon. Technol. Lett.*, vol. 31, no. 10, pp. 799–802, May 2019.
[15] M. G. Saber *et al.*, "DSP-free 25 Gb/s PAM-4 transmission using 10 G transmitter and coherent amplification," *IEEE Photon. Technol. Lett.*, vol. 30, no. 17, pp. 1547–1550, Sep. 2018.
[16] A. Napoli *et al.*, "Digital pre-compensation techniques enabling high-capacity bandwidth variable transponders," *Opt. Commun.*, vol. 409, pp. 52–65, 2018.
[17] A. Khilo, C. M. Sorace, and F. X. Kärtner, "Broadband linearized silicon modulator," *Opt. Exp.*, vol. 19, no. 5, pp. 4485–4500, 2011.
[18] G. Khanna *et al.*, "A memory polynomial based digital pre-distorter for high power transmitter components," in *Proc. Opt. Fiber Commun. Conf.*, 2017, Art. no. M2C-4.
[19] A. Lender, "Correlative digital communication techniques," *IEEE Trans. Commun. Technol.*, vol. COM-12, no. 4, pp. 128–135, Dec. 1964.
[20] D. Van Veen, V. Houtsma, and H. Chow, "Demonstration of symmetrical 25 Gbps quaternary PAM/Duobinary TDM-PON with multilevel interleaving of users," in *Proc. IEEE Opt. Commun., Eur. Conf.*, 2015, pp. 1–3.
[21] P. Torres-Ferrera, H. Wang, V. Ferrero, and R. Gaudino, "100 Gbps/λ PON downstream O- and C-band alternatives using direct-detection and linear-impairment equalization," *IEEE/OSA J. Opt. Commun. Netw.*, vol. 13, no. 2, pp. A 111-A123, Feb. 2021.
[22] L. F. Suhr, J. V. Olmos, B. Mao, X. Xu, G. Liu, and I. T. Monroy, "112-Gbit/s$\times$ 4-lane duobinary-4-PAM for 400GBase," in *Proc. IEEE Eur. Conf. Opt. Commun.*, 2014, pp. 1–3.
[23] M. G. Saber *et al.*, "100 Gb/s/λ duo-binary PAM-4 transmission using 25 G components achieving 50 km reach," *IEEE Photon. Technol. Lett.*, vol. 32, no. 3, pp. 138–141, Feb. 2020.
[24] J. Zhang *et al.*, "280 Gb/s IM/DD PS-PAM-8 transmission over 10 km SSMF at o-band for optical interconnects," in *Proc. Opt. Fiber Commun. Conf.*, 2020, Art. no. M4F-1.
[25] D. Kim, Z. He, T. Bo, Y. Yu, and H. Kim, "Transmission of 36-Gbaud PAM-8 signal in IM/DD system using pairwise-distributed probabilistic amplitude shaping," in *Proc. IEEE Opt. Fiber Commun. Conf. Exhib.*, 2020, pp. 1–3.
[26] N.-P. Diamantopoulos, W. Kobayashi, H. Nishi, K. Takeda, T. Kakitsuka, and S. Matsuo, "Amplifierless PAM-4/PAM-8 transmissions in O-band using a directly modulated laser for optical data-center interconnects," *Opt. Lett.*, vol. 44, no. 1, pp. 9–12, 2019.
[27] C. Prodaniuc, N. Stojanovic, C. Xie, Z. Liang, J. Wei, and R. Llorente, "3-dimensional PAM-8 modulation for 200 Gbps/lambda optical systems," *Opt. Commun.*, vol. 435, pp. 1–4, 2019.
[28] G. P. Agrawal, *Fiber-Optic Communication Systems*, 3rd ed. Hoboken, NJ, USA: Wiley, 2002.
[29] G. Jacobsen, K. Bertilsson, and Z. Xiaopin, "WDM transmission system performance: Influence of non-Gaussian detected ASE noise and periodic DEMUX characteristic," *J. Lightw. Technol.*, vol. 16, no. 10, pp. 1804–1812, 1998.
[30] *Media Access Control Parameters, Physical Layers, and Management Parameters for 40 Gb/s and 100 Gb/s Operation*, IEEE Standard 802.3ba, *IEEE Comput. Soc.*, 2010.
[31] "FEC Code for 25/50/100 G EPON," 2017. [Online]. Available: https://www.ieee802.org/3/ca/public/meeting_archive/2017/03/vanveen_3ca_1b_0317.pdf
[32] A. Papoulis and S. U. Pillai, *Probability, Random Variables and Stochastic Processes*, 4th ed. New York, NY, USA: McGraw-Hill, 2002.
[33] R. Stephens, M. Mueller, and R. McHugh, "Total jitter measurement at low probability levels using optimized BERT scan method," *Agilent Technol., White Paper*, 2005.